Phase diagrams of binary mixtures of patchy colloids with distinct numbers and types of patches: The empty fluid regime

Daniel de las Heras,[1,a)] José Maria Tavares,[1,2,b)] and Margarida M. Telo da Gama[1,3,c)]

[1]*Centro de Física Teórica e Computacional da Universidade de Lisboa, Avenida Professor Gama Pinto 2, P-1749-016, Lisbon, Portugal*
[2]*Instituto Superior de Engenharia de Lisboa, Rua Conselheiro Emíidio Navarro, P-1590-062, Lisbon, Portugal, and Centro de Física Teórica e Computacional da Universidade de Lisboa, Avenida Professor Gama Pinto 2, P-1749-016, Lisbon, Portugal*
[3]*Departamento de Física, Facultade de Ciências da Universidade de Lisboa, Campo Grande, P-1749-016, Lisbon, Portugal*

We investigate the effect of distinct bonding energies on the onset of criticality of low functionality fluid mixtures. We focus on mixtures of particles with two and three patches as this includes the mixture where "empty" fluids were originally reported. In addition to the number of patches, the species differ in the type of patches or bonding sites. For simplicity, we consider that the patches on each species are identical: one species has three patches of type A and the other has two patches of type B. We have found a rich phase behavior with closed miscibility gaps, liquid–liquid demixing, and negative azeotropes. Liquid–liquid demixing was found to pre-empt the "empty" fluid regime, of these mixtures, when the AB bonds are weaker than the AA or BB bonds. By contrast, mixtures in this class exhibit "empty" fluid behavior when the AB bonds are stronger than at least one of the other two. Mixtures with bonding energies $\epsilon_{BB} = \epsilon_{AB}$ and $\epsilon_{AA} < \epsilon_{BB}$, were found to exhibit an unusual negative azeotrope. © *2011 American Institute of Physics*. [doi:10.1063/1.3561396]

I. INTRODUCTION

In the last twenty years the study of colloidal phase diagrams, based on spherically symmetric particle interactions, revealed a rich phenomenology including new crystal phases, gelation, and glass transitions.[1,2] The phase behavior of binary mixtures is richer and colloidal binary mixtures are expected to have a wider range of applications in technology as well as in biology. Examples include novel candidate photonic crystals, synthesized by van Blaaderen and co-workers, through fine control of the colloidal charges[3] (see also the simulations of Ref. 4), and binary mixtures of eye-lens proteins, studied by Schurtenberger *et al.*, where attractive unlike (spherical) interactions were found to be crucial to stabilize the mixture, a mechanism relevant in the prevention of cataract formation.[5]

Nowadays colloidal particles can be synthesized in a range of shapes and their surfaces may be functionalized in a variety of ways,[6–10] with the result that the particle interactions become directional or "patchy." The primitive model of patchy colloids consists of hard-spheres (HSs) with f patches on their surfaces. Patchy particles attract each other if and only if two of their patches overlap. The attraction between particles is short ranged and anisotropic: the patches act as bonding sites and promote the appearance of well defined clusters, whose structure and size distribution depend on the properties of the patches (f and the bonding energy) and on the thermodynamic conditions (density and temperature).

Sciortino and co-workers established that f, the number of patches or bonding sites per particle, is the key parameter controlling the location of the liquid–vapor (LV) critical point.[11,12] They showed that, for low values of f (approaching 2), the phase separation region is drastically reduced, and low densities and temperatures can be reached without encountering the phase boundary. These low density ("empty") phases were shown to be network liquids, suggesting that, on cooling, patchy particles could assemble into a glassy state of arbitrary low density (a gel). Very recently, Ruzicka and co-workers have reported the first experimental evidence of empty liquids in dilute suspensions of Laponite.[13] Their properties were found to be similar to those predicted by the primitive patchy colloidal models.

Remarkably, the results of the simulations of patchy colloidal particles are well described by classical liquid state theories: Wertheim's first order perturbation theory[14–17] predicts correctly the equilibrium thermodynamic properties; Flory–Stockmayer[18–20] theories of polymerization describe quantitatively the size distributions of the clusters of patchy particles, including the appearance of network (percolated) fluids.

In subsequent work we addressed, explicitly, the interplay of the entropy of mixing and the entropy of bonding in the phase behavior of models of binary mixtures of patchy particles. We focused on mixtures of particles which differ in the number of patches or functionality only. We found that, within this class of mixtures, the difference between the functionality of the particles is the key parameter controlling the phase equilibria of the system. In particular, if one species has more than twice the number of bonding sites of the other, a phase transition between two network fluids appears and the

a)Electronic mail: delasheras.daniel@gmail.com.
b)Electronic mail: josemaria.castrotavares@gmail.com.
c)Electronic mail: margarid@cii.fc.ul.pt.

134, 104904-1

topology of the phase diagram may change. The miscibility at high pressures is also controlled by this difference and closed miscibility gaps are always present when the difference, between the functionality of the particles, is greater than one.[21] The conditions required to realize empty phases were shown to differ from those proposed by Sciortino and co-workers, and no "empty" liquids were found when the functionality of one of the species exceeds 4.[21]

The primitive model of patchy particles was generalized to include different types of patches (i.e., more than one bonding energy). This was achieved[22–24] by considering a single component fluid where the particles have two A sites (with bonding energy ϵ_{AA}), and one B site (with bonding energy ϵ_{BB}). Unlike sites also interact with bonding energy ϵ_{AB}. This model allows a deeper understanding of the onset of criticality in low functionality systems: the detailed fashion in which the critical temperature vanishes, as the bonding energies decrease toward zero, depends on the order in which the limits are taken, which, in turn, determines the type of the network that is formed. Empty phases are low-density structured (percolated) fluids and the emergence of criticality is related to this structure. Thus, the generalized model provides a reference system for the microscopic description of the competition between condensation and self-assembly of equilibrium structured fluids as the theoretical predictions based on Wertheim's theory have been confirmed, recently, by Monte Carlo simulations.[25,26]

In the present work, we proceed to investigate the effect of distinct bonding energies on the onset of criticality of low functionality fluid mixtures. We focus on mixtures of particles with two and three patches as this is the type of mixture where empty fluids were originally reported. In addition to the number of patches the species may differ in the type of patches or bonding sites. For simplicity, we assume that the patches on each species are identical, i.e., we consider mixtures of particles with two B patches and particles with three A patches: $2_B - 3_A$ mixtures.

As for pure fluids, we will use Wertheim's thermodynamic perturbation theory (in its extension to mixtures)[27] and Flory–Stockmayer's theory of percolation (generalized to mixtures[21]). The colloids are modeled by equisized hard spheres and we vary the strength of the bonding energies ϵ_{AA}, ϵ_{BB}, and ϵ_{AB} (Fig. 1). We recover the $2_A - 3_A$ mixture investigated previously[11,21] when all bonding energies are equal. This is a type I mixture that is completely miscible above the critical pressure of the less volatile component. The empty

fluid regime is approached monotonically: the critical packing fraction and the temperature decrease toward zero as the fraction of 2_A particles approaches one (i.e., the average functionality decreases toward two).

We found a rich phase behavior with closed miscibility gaps, liquid–liquid (LL) demixing, negative azeotropes, and, from a topological point of view, three different types of mixtures: type I, I-A, and III.[28] Liquid–liquid demixing is the mechanism which prevents this class of mixtures from exhibiting empty fluid behavior and this occurs when the AB bonds are weaker than the AA or BB bonds. By contrast, the mixtures exhibit empty fluid behavior when the AB bonds are stronger than at least one of the other two. Furthermore, mixtures with bonding energies $\epsilon_{BB} = \epsilon_{AB}$ and $\epsilon_{AA} < \epsilon_{BB}$, exhibit an unusual (negative) azeotropic behavior.

We found an exception where the AB bonds are stronger but the mixture fails to exhibit empty fluid behavior: the mixture with $\epsilon_{AB} = \epsilon_{AA}$ and $\epsilon_{BB} = 0$. Near the critical point of this mixture there is demixing and two network fluids with a finite packing fraction coexist, as the pressure vanishes. This behavior resembles that found previously[21] for $2_A - 5_A$ mixtures where the entropy of bonding drives a demixing transition, which pre-empts the empty fluid liquid–vapor phase transition.

The remainder of the paper is organized as follows. In Sec. II, we present the model, summarize Wertheim's theory for binary mixtures (Sec. II A), and the Flory–Stockmayer theory of percolation for binary mixtures of patchy particles (Sec. II B). In Sec. III, we present the results: phase diagrams (including percolation lines) and critical properties of several representative mixtures. Finally, in Sec. IV, we summarize our conclusions and suggest lines for future research.

II. MODEL AND THEORY

We consider a binary mixture of N_1 and N_2 equisized HSs with diameter σ. Particles of species 1 are decorated with two patches of type B, and particles of species 2 with three patches of type A: a $2_B - 3_A$ binary mixture. The bonding sites are distributed on the particle surfaces in such a manner that two particles can form only one single bond, involving two bonding sites only, one in each particle. In addition, there is a minimum distance between the bonding sites to ensure that no sites are shaded by nearby bonds.

A. Helmholtz free energy: Wertheim's thermodynamic perturbation theory

A description of Wertheim's perturbation theory for pure fluids and mixtures can be found elsewhere.[14–17,27] Here we summarize the theory for the mixture under consideration (the theory for binary mixtures with an arbitrary number of patches of different types is discussed in Ref. 21).

The Helmholtz free energy per particle, f_H, is the sum of contributions from a reference system, a mixture of hard spheres (f_{HS}), and a perturbation due to the bonding interactions (f_b):

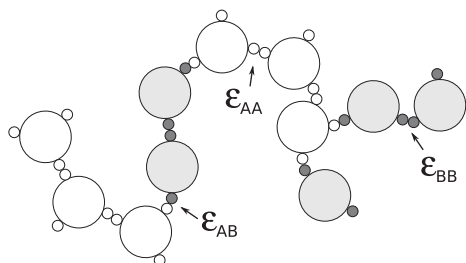$$f_H = F_H/N = f_{HS} + f_b, \qquad (1)$$

FIG. 1. Schematic representation of the mixture under consideration illustrating the different bonding energies.

where $N = N_1 + N_2$ is the total number of particles. The HSs free energy may be written as the sum of ideal-gas and excess contributions: $f_{HS} = f_{id} + f_{ex}$. The ideal-gas free energy is given by

$$\beta f_{id} = \ln \eta - 1 + \sum_{i=1,2} x^{(i)} \ln(x^{(i)} \mathcal{V}_i) \qquad (2)$$

with $\beta = 1/kT$ being the inverse thermal energy, $\mathcal{V}_i$ being the thermal volume, and $x^{(i)} = N_i/N$ being the number fraction of each species. $\eta = v_s \rho$ is the total packing fraction, $v_s = \pi/6\sigma^3$ is the volume of a single particle, and ρ is the total number density. The excess part, which includes the effect of the excluded volume, is approximated by the Carnahan–Starling equation of state[29] (note that both species have the same diameter):

$$\beta f_{ex} = \frac{4\eta - 3\eta^2}{(1-\eta)^2}. \qquad (3)$$

The bonding free energy has two contributions: the bonding energy and an entropic term related to the number of ways of bonding two particles. In the framework of Wertheim's thermodynamic first-order perturbation theory it is given by[21,27]

$$\beta f_b = x \left[2 \ln X_B - X_B + 1 \right] + (1 - x)$$
$$\times \left[3 \ln X_A - \frac{3}{2} X_A + \frac{3}{2} \right], \qquad (4)$$

where $x \equiv x^{(1)}$ is the composition of the mixture ($x^{(2)} = 1 - x$) and X_α is the probability that a site of type $\alpha = A, B$ is *not* bonded. The latter are related to the thermodynamic quantities through the law of mass action:

$$X_A = 1 - 2\eta x X_B X_A \Delta_{AB} - 3\eta(1-x) X_A^2 \Delta_{AA},$$
$$X_B = 1 - 2\eta x X_B^2 \Delta_{BB} - 3\eta(1-x) X_A X_B \Delta_{AB}. \qquad (5)$$

The set of parameters $\Delta_{\alpha\gamma}$ characterize the bonds between sites α and γ. For simplicity, the interaction between bonding sites is modeled by square well potentials with depths $\epsilon_{\alpha\gamma}$. Assuming that all bonds have the same volume, v_b, and using the ideal-gas approximation for the pair correlation function of the reference HS fluid, we find[21]

$$\Delta_{\alpha\gamma} = \frac{v_b}{v_s} [\exp(\beta \epsilon_{\alpha\gamma}) - 1]. \qquad (6)$$

As in previous works,[22,23] we set the bond volume to $v_b = 0.000332285\sigma^3$. We consider mixtures where two of the three bonding energies, ϵ_{AA}, ϵ_{AB}, and ϵ_{BB}, are equal and vary the third. The two identical energies set the energy scale, ϵ. In what follows we use scaled-bonding energies $\epsilon_{\alpha\gamma}^* = \epsilon_{\alpha\gamma}/\epsilon$.

We use the Gibbs free energy per particle ($g = p/\rho + f_H$, where p is the pressure) to obtain the equilibrium properties of the mixture. At fixed values of the composition x, pressure p, and temperature T, g is minimized with respect to the total density ρ, subject to the constraints imposed by the law of mass action. We use a standard Newton–Raphson method to minimize g, and solve the law of mass action simultaneously by a Powell hybrid method.

A standard common tangent construction on $g(x)$ is used to determine the coexistence points (which is equivalent to

imposing the equality of the chemical potentials in the coexisting phases), while mechanical and thermal equilibria are satisfied by fixing the pressure and the temperature, respectively.

Finally, the critical points are computed numerically by determining the states which satisfy the spinodal condition and the vanishing of the third-order derivative in the direction of largest growth.[30]

B. Theory of percolation

Recently,[21] we generalized an extension of the Flory–Stockmayer random-bond percolation theory[18–20] proposed by Tavares *et al.*[25] to binary mixtures with an arbitrary number of distinct bonding sites. Consider a treelike cluster (i.e., with no loops) as schematically illustrated in Fig. 2. The number of bonded sites α at the level $i + 1$ is related to the number of all types of bonded sites in the previous level through the recursion relations (see Refs. 21 and 25 for details):

$$n_{i+1,A} = 2p_{A \to A} n_{i,A} + p_{B \to A} n_{i,B},$$
$$n_{i+1,B} = 2p_{A \to B} n_{i,A} + p_{B \to B} n_{i,B}, \qquad (7)$$

where $p_{\alpha \to \gamma}$ is the probability of bonding a site α to a site γ. Then, the probability of finding a bonded site α is

$$P_A = p_{A \to A} + p_{A \to B},$$
$$P_B = p_{B \to A} + p_{B \to B}, \qquad (8)$$

which may be related to the thermodynamic quantities through the law of mass action, since

$$P_\alpha = 1 - X_\alpha, \quad \alpha = A, B. \qquad (9)$$

A term-by-term analysis of Eqs. (5) and (8) gives

$$p_{A \to A} = (1-x)3\eta X_A^2 \Delta_{AA},$$
$$p_{A \to B} = x2\eta X_A X_B \Delta_{AB},$$
$$p_{B \to B} = x2\eta X_B^2 \Delta_{BB},$$
$$p_{B \to A} = (1-x)3\eta X_A X_B \Delta_{AB}. \qquad (10)$$

In order to find whether the system is percolated or not, we write Eq. (7) in matrix form:
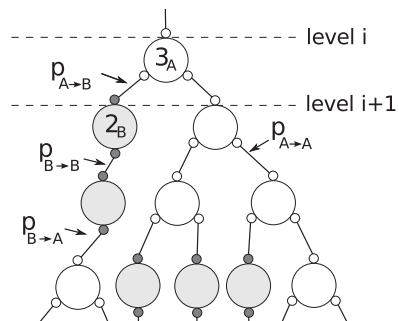
$$\tilde{n}_i = \tilde{T}^i \tilde{n}_0, \qquad (11)$$

FIG. 2. Schematic representation of a treelike cluster in a $2_B - 3_A$ binary mixture. $p_{\alpha \to \gamma}$ is the probability of bonding a site α to a site γ.
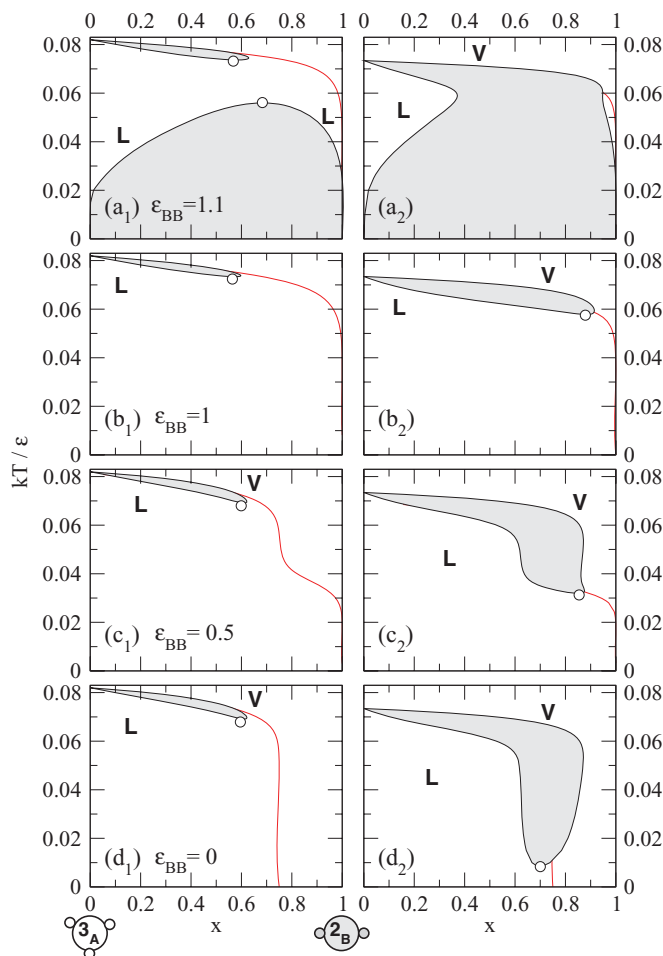
FIG. 3. Phase diagrams of mixtures of particles with two patches of type B (species 1) and three patches of type A (species 2) in the scaled-temperature vs composition ($x = x^{(1)}$) plane at constant pressure. The bonding interactions are: $\epsilon_{AA}^* = \epsilon_{AB}^* = 1$ and: row 1 (a_1) and (a_2) $\epsilon_{BB}^* = 1.1$, (b_1) and (b_2) $\epsilon_{BB}^* = 1$, (c_1) and (c_2) $\epsilon_{BB}^* = 0.5$, (d_1) and (d_2) $\epsilon_{BB}^* = 0$. Left column: Pressure $p_1^* = p_1 v_s/\epsilon = 1.05 \times 10^{-4}$, Right column: Pressure $p_2^* = p_2 v_s/\epsilon = 1.05 \times 10^{-5}$.

where $\tilde{n}_i$ is a vector with components $n_{i,\alpha}$ and $\tilde{T}$ is a 2×2 square matrix with entries

$$\tilde{T} = \begin{pmatrix} 2p_{A \to A} & p_{B \to A} \\ 2p_{A \to B} & p_{B \to B} \end{pmatrix}, \quad (12)$$

which may be diagonalized. The progressions defined by Eq. (11) converge to 0 if the largest (absolute value) of the eigenvalues of $\tilde{T}$ is less than unity. In other words, percolation occurs when $|\lambda_\pm| = 1$ for any of the two eigenvalues $\lambda_\pm$ of $\tilde{T}$.

III. RESULTS

Before describing the results for $2_A - 3_A$ mixtures we set the graphical code/s used in the figures. Phase diagrams are presented, in the temperature-composition plane at constant pressure, in Figs. 3, 6, and 9. In all the figures percolation lines are plotted as solid red lines: below the percolation line the fluid is percolated in the sense that there is a nonzero probability of finding an infinite cluster. We call these
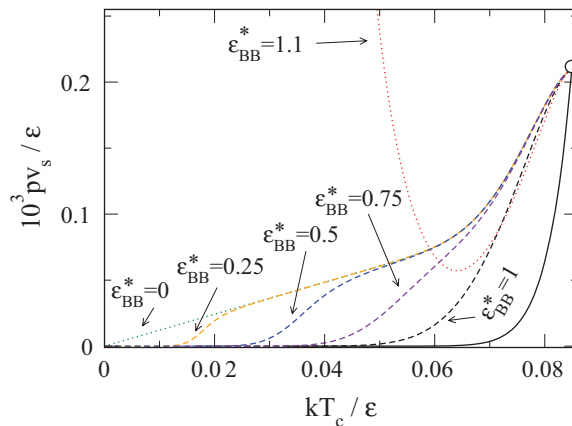

FIG. 4. Pressure–temperature projections of the phase diagrams of binary mixtures with $\epsilon_{AA}^* = \epsilon_{AB}^* = 1$. The solid curve is the liquid–vapor transition of the pure 3_A fluid, which ends in a critical point (open circle). Dashed and dotted lines are the critical lines of the mixture.

networks fluids. The liquid side/s of the binodal lines is/are always percolated; binodal lines are depicted as black solid lines; shaded areas are two-phase regions; empty circles are critical points; black squares are azeotropic points.

The critical properties of the mixtures are analyzed by means of pressure–temperature projections (Figs. 4, 7, and 10) and critical temperature versus critical packing fraction representations (Figs. 5, 8, and 11). In all cases, solid lines depict the liquid–vapor transition and empty circles depict the critical point of the pure fluid (3_A fluid). Dashed and dotted lines are the critical points of the mixture: when the mixture exhibits empty fluid behavior, at low pressure, the critical line is dashed, otherwise it is shown dotted.

A. $2_A - 3_A$ mixture

We start by reviewing the results for the mixture with identical bonding interactions, which was investigated by grand-canonical Monte Carlo simulations[11] and using the current theory.[21] At low pressures, the pure 3_A fluid undergoes LV liquid–vapor condensation, below the critical temperature. The transition involves two fluids with different densities and fraction of unbonded sites. By contrast, there is no
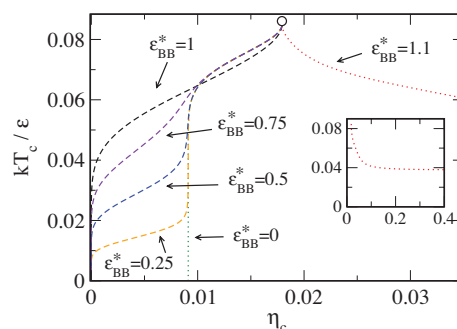

FIG. 5. Scaled-critical temperature vs critical packing fraction of mixtures with $\epsilon_{AA}^* = \epsilon_{AB}^* = 1$. The open circle denotes the critical point of the pure 3_A fluid. The inset is a zoom of the case $\epsilon_{BB}^* = 1.1$, where $\eta_c \to 1$.
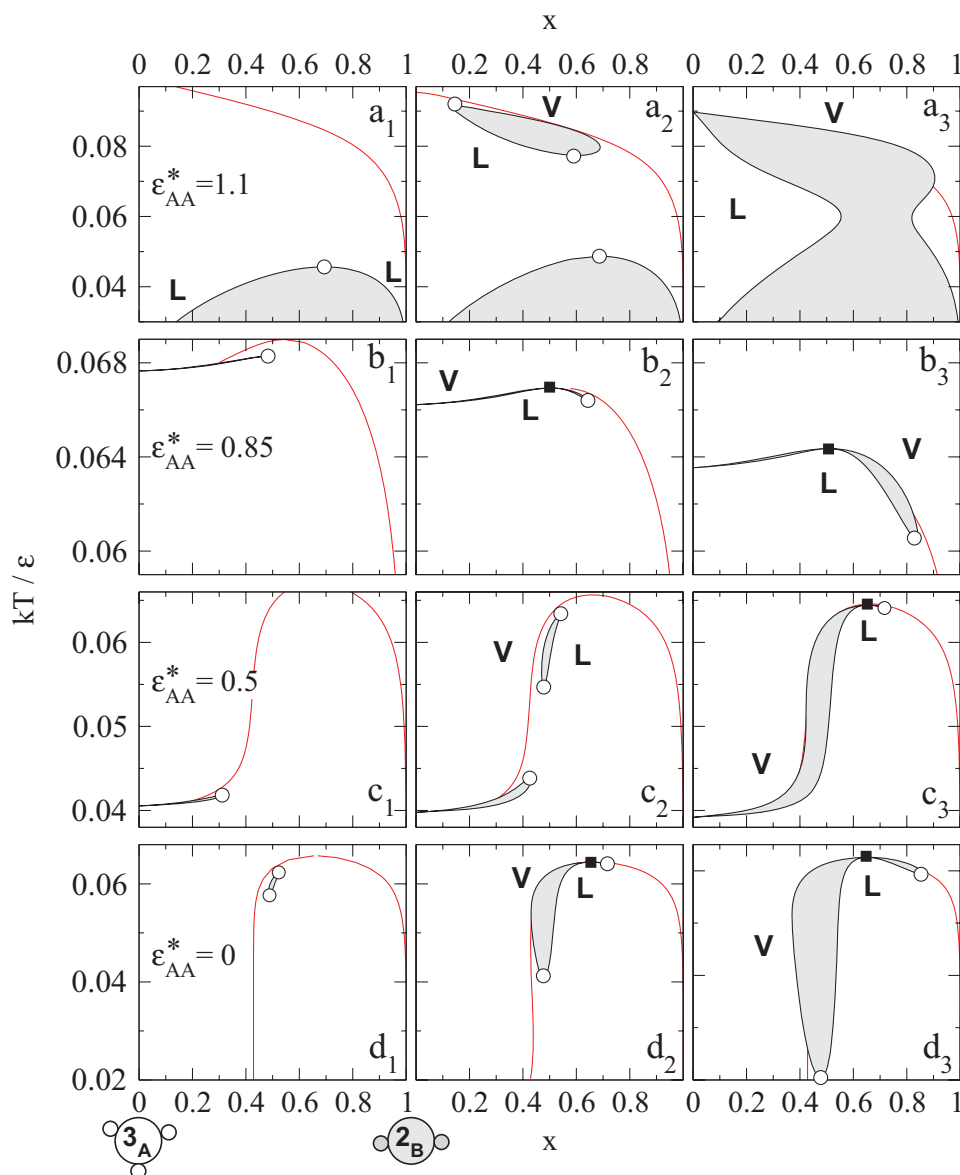
FIG. 6. Phase diagrams in the scaled-temperature vs composition ($x = x^{(1)}$) plane at constant pressure of $2_B - 3_A$ binary mixtures with $\epsilon^*_{AB} = \epsilon^*_{BB} = 1$. First row: $\epsilon^*_{AA} = 1.1$, pressures: $p^* = pv_s/\epsilon = 5.24 \times 10^{-4}$ (a_1), $p^* = 3.14 \times 10^{-4}$ (a_2), $p^* = p^*_1 = 1.05 \times 10^{-4}$ (a_3). Second row: $\epsilon^*_{AA} = 0.85$, pressures: $p^* = 5.24 \times 10^{-5}$ (b_1), $p^* = 3.14 \times 10^{-5}$ (b_2), $p^* = 1.31 \times 10^{-5}$ (b_3). Third row: $\epsilon^*_{AA} 0.5$, pressures: $p^* = 4.19 \times 10^{-5}$ (c_1), $p^* = 2.83 \times 10^{-5}$ (c_2), $p^* = 2.09 \times 10^{-5}$ (c_3). Fourth row: $\epsilon^*_{AA} = 0$, pressures: $p^* = 2.88 \times 10^{-5}$ (d_1), $p^* = 2.09 \times 10^{-5}$ (d_2), $p^* = p^*_2 = 1.05 \times 10^{-5}$ (d_3).

LV transition in the pure 2_A fluid, as the particles with two bonding sites can form linear chains only and the absence of branching prevents the fluids from condensing. For the mixture, the simulation and theoretical results indicate that the critical packing fraction decreases continuously toward zero as the pressure vanishes, exhibiting empty liquid behavior, that is, there is a fluid phase with an arbitrary low packing fraction.

The temperature-composition phase diagrams are illustrated in Fig. 3 panels (b_1) and (b_2) at two distinct pressures below $p^{(3)}_c$, the critical pressure of the pure 3_A fluid (the mixture is completely miscible above $p^{(3)}_c$). When 2_A particles are added the LV phase transition shifts from $x = 0$ (3_A fluid) to finite values of the composition. The two-phase region, which is always bounded by a lower critical point, increases as the

pressure decreases. Near the $x = 0$ axis the slope of the binodal is negative, indicating a decrease in the stability of the liquid phase as the fraction of 2_A particles increases. The addition of 2_A particles reduces the probability of branching, the mechanism which drives condensation, and consequently the region of stability of the liquid phase decreases.

The pT projection of the critical line (see Fig. 4) starts at the critical point of the less volatile fluid (3_A fluid) and decreases monotonically to $p \to 0$ and $T \to 0$. Topologically this is a limiting case of type I mixtures, with no liquid–liquid demixing, according to the classification of van Konynenburg and Scott,[28] where one of the fluids does not undergo LV condensation (2_A fluid).

In what follows, we consider generic $2_B - 3_A$ mixtures (i.e., where species 1 is decorated with two patches of type B
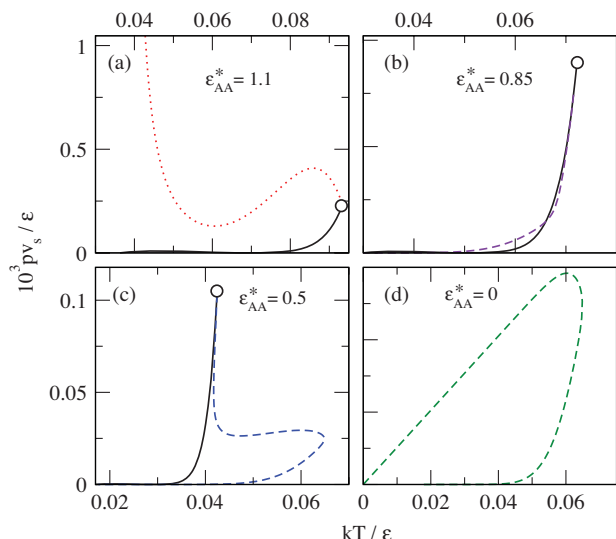
FIG. 7. Pressure–temperature projections of the phase diagrams of different binary mixtures with $\epsilon_{AB}^* = \epsilon_{BB}^* = 1$.

and species 2 with three patches of type A) which are characterized by three bonding interactions: ϵ_{AA}^*, ϵ_{BB}^*, and ϵ_{AB}^*. We proceed by setting, in turn, two of them equal and vary the third.

B. $2_B - 3_A$ mixtures: $\epsilon_{AA} = \epsilon_{AB}$

We start by setting $\epsilon_{AA}^* = \epsilon_{AB}^* = 1$. Tx phase diagrams are depicted in Fig. 3 at two different pressures: $p_1^* = p_1 v_s / \epsilon = 1.05 \times 10^{-4}$ (left column) and $p_2^* = 1.05 \times 10^{-5}$ (right column), both below $p_c^{(3)}$, the critical pressure of the pure 3_A fluid. pT projections are plotted in Fig 4 and critical properties are illustrated in Fig. 5.

1. $\epsilon_{BB}^* > 1$, $\epsilon_{AA}^* = \epsilon_{AB}^* = 1$

When $\epsilon_{BB}^* > 1$, there is liquid–liquid demixing at low temperature for any value of the pressure. The demixing involves two structured (percolated) fluids: one rich in 3_A particles, and the other rich in 2_B particles. The phase
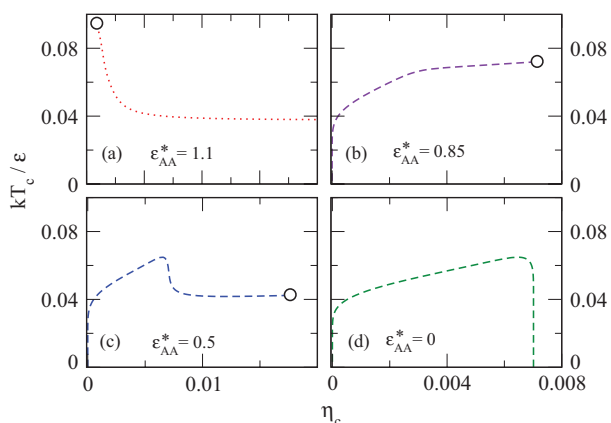

FIG. 8. Scaled-critical temperature vs critical packing fraction in mixtures with $\epsilon_{AB}^* = \epsilon_{BB}^* = 1$.
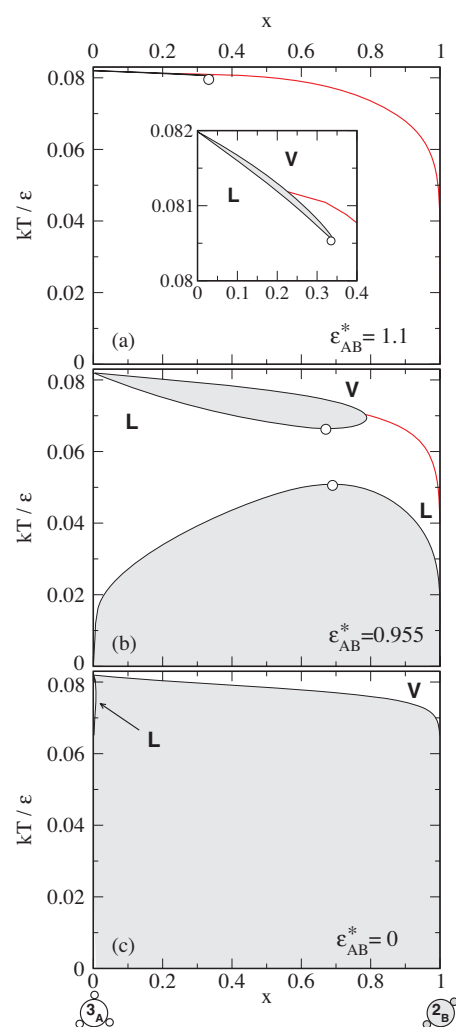

FIG. 9. Phase diagrams of $2_B - 3_A$ binary mixtures in the scaled-temperature vs composition plane at constant pressure $p_1^* = p v_s / \epsilon = 1.05 \times 10^{-4}$. In all cases $\epsilon_{AA}^* = \epsilon_{BB}^* = 1$. $\epsilon_{AB}^* = 1.1$ (a), $\epsilon_{AB}^* = 0.955$ (b), and $\epsilon_{AB}^* = 0$ (c). The inset in (a) is a zoom of the two-phase region.

separation is driven by the presence of AB bonds as they reduce the number of BB bonds which are energetically favorable. The demixing at low temperatures pre-empts the empty fluid regime.

We chose $\epsilon_{BB}^* = 1.1$ as a representative example of this class of mixtures. At pressures higher than $p_c^{(3)}$ the Tx phase diagram (not shown) consists in a demixing region bounded above by an upper critical point. Sightly below $p_c^{(3)}$ there are two regions of phase separation bounded by critical points [panel (a$_1$) of Fig. 3]: LL demixing at low temperatures and LV at high temperatures. By reducing the pressure below a certain value ($p/p_c^{(3)} \approx 0.27$), the two regions merge giving rise to a very large demixing region without critical points [panel (a$_2$) of Fig. 3].

The pure 2_B fluid does not undergo LV condensation, and thus the phase diagram of these mixtures does not fit exactly the standard classification of van Konynenburg and Scott.[28] Nevertheless, it may be understood as a limiting case of type III mixtures (see the pT projection in Fig. 4). The critical line, which changes its character continuously from LV to LL, starts at the critical point of the less volatile fluid,
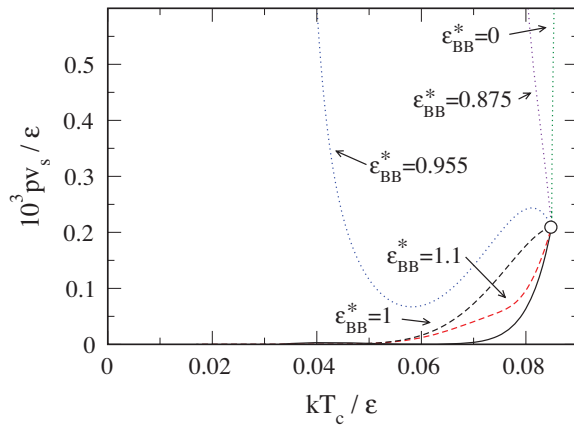
FIG. 10. Pressure–temperature projections of the phase diagrams of binary mixtures with $\epsilon_{AA}^* = \epsilon_{BB}^* = 1$.

exhibits a minimum, and continues with a negative slope to high pressures. This line is expected to intersect the solid phase boundaries that were not considered here. The topology of the phase diagram remains the same for other mixtures with $\epsilon_{BB}^* > 1$, but changes in the critical line, such as the absence of the minimum, may occur.

The critical temperature and the packing fraction are plotted in Fig. 5. As the pressure increases the packing fraction increases while the critical temperature and concentration tend asymptotically to $kT_c/\epsilon \to 0.037$ and $x_c \to 0.757$.

2. $\epsilon_{BB}^* = 0$, $\epsilon_{AA}^* = \epsilon_{AB}^* = 1$

Let us continue by considering the extreme case where the B patches do not interact: $\epsilon_{BB}^* = 0$. The mixture is completely miscible at pressures above $p_c^{(3)}$. Slightly below $p_c^{(3)}$ the Tx phase diagrams [an example is plotted in panel (d$_1$) of Fig. 3] are similar to those of the reference mixture ($2_A - 3_A$): the LV phase transition shifts from $x = 0$ (3_A fluid) to finite values of the composition. The differences appear at lower temperatures. As a result of the absence of bonding between 2_B particles, there is no condensation when the fraction of 2_B particles in the mixture is sufficiently large. When the tem-
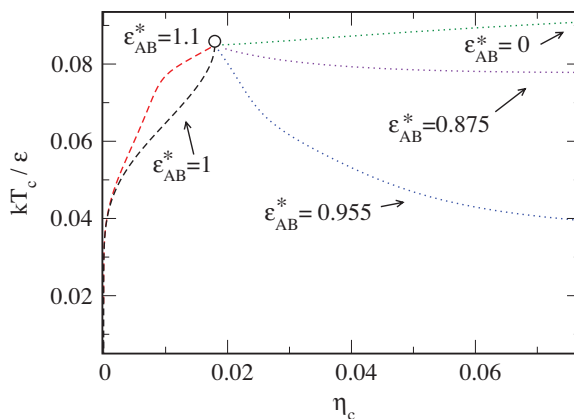

FIG. 11. Scaled-critical temperature vs critical packing fraction of binary mixtures with $\epsilon_{AA}^* = \epsilon_{BB}^* = 1$. In all cases with $\epsilon_{AB}^* < 1$ the critical packing fraction tends to $\eta_c \to 1$.

perature decreases, at any value of the pressure, the percolation line tends asymptotically to $x \to 0.75$ (with $X_A \to 0$ and $X_B \to 0.5$) rather than $x \to 1$ (with $X_A \to 0$ and $X_B \to 0$) as in the reference mixture. Differences in the phase diagrams are noticeable as the pressure is further reduced [see panel (d$_2$) in Fig. 3]. Near $x = 0$, there is a LV transition similar to the transition of the reference mixture, but as the temperature is lowered, the two-phase region changes drastically and ends in a lower critical point. Topologically, this is still a limiting case of type I mixtures (pT projection is depicted in Fig. 4). The critical temperature approaches zero when the pressure vanishes, as in the reference mixture, but the critical packing fraction tends asymptotically to $\eta_c = 0.0091$ (see Fig. 5) and $x_c \to 0.699$ rather than $\eta_c \to 0$ and $x_c \to 1$. Thus, there is no empty liquid regime when the B patches do not interact. The difference between the AA and BB bonding energies drives demixing between two network fluids, which pre-empts the LV phase transition at low pressures.

3. $0 < \epsilon_{BB}^* < 1$, $\epsilon_{AA}^* = \epsilon_{AB}^* = 1$

These mixtures retain features of the previous two classes, those with $\epsilon_{BB}^* = 1$ and those with $\epsilon_{BB}^* = 0$. An example of the temperature-composition phase diagrams at constant pressure is shown in the third row of Fig. 3 for $\epsilon_{BB}^* = 0.5$, examples of the pT projections are depicted in Fig. 4, and the critical properties are illustrated in Fig. 5.

At intermediate temperatures, the BB interactions are frozen (in the sense that the probability of BB bonding is much smaller than the probability of AB or AA bonding) and the mixture behaves as the mixture with $\epsilon_{BB} = 0$. Eventually, at low enough temperatures, all bonds are established and the mixture behaves as the reference $2_A - 3_A$ mixture. In particular, the empty liquid regime ($T_c \to 0$ and $\eta_c \to 0$ as the pressure vanishes) is observed. In all cases these mixtures are limiting cases of type I phase equilibria where only one component undergoes LV condensation.

C. $2_B - 3_A$ mixtures: $\epsilon_{AB} = \epsilon_{BB}$

We continue the analysis by setting $\epsilon_{AB}^* = \epsilon_{BB}^* = 1$ and varying the bonding energy of AA bonds.

1. $\epsilon_{AA}^* > \epsilon$, $\epsilon_{AB}^* = \epsilon_{BB}^* = 1$

We selected $\epsilon_{AA}^* = 1.1$ to illustrate the behavior of this class of mixtures. Temperature-composition phase diagrams at different pressures are plotted in Fig. 6 (a$_1$) $pv_s/\epsilon = 5.24 \times 10^{-4}$ (well above the critical pressure of the pure substance $p_c^{(3)}$), (a$_2$) $pv_s/\epsilon = 3.142 \times 10^{-4}$ (slightly above $p_c^{(3)}$), and (a$_3$) $p_1^* = pv_s/\epsilon = 1.05 \times 10^{-4}$ (slightly below $p_c^{(3)}$). The behavior is similar to the mixture with $\epsilon_{BB}^* = 1.1$ and $\epsilon_{AB}^* = \epsilon_{AA}^* = 1$, analyzed in Sec. III B 1. In addition to the LV condensation, there is a LL demixing region at low temperatures for any value of pressure. Well above $p_c^{(3)}$ the LL demixing region is bounded by an upper critical point, Fig. 6 (a$_1$). As $p_c^{(3)}$ is approached from above, the LV condensation appears in the form of closed loops of immiscibility (a$_2$). By further reducing the pressure, the two-phase regions grow and

eventually merge giving rise to a very large demixing region, which intersects the $x = 0$ axis at the temperature of the LV transition of the pure component (a$_3$). The percolation analysis shows that liquid phases are always network fluids while the vapor phase may or may not be percolated. Closed loops of immiscibility, when present, are entirely percolated.

The origin of the LL demixing at low temperatures is the same as that observed in the mixtures with $\epsilon_{BB}^* = 1.1$ and $\epsilon_{AB}^* = \epsilon_{AA}^* = 1$. As the temperature is reduced the fractions of unbonded sites, X_A and X_B, decrease and there is demixing between a phase where the AA bonds are predominant (small values of composition) and another where the BB bonds predominate (large values of composition). AB bonds are penalized as they reduce the probability of AA bonding, which is energetically favorable.

This mixture is topologically classified as a limiting case of type III phase equilibria [(see the pT projection in Fig. 7(a)] where only one fluid undergoes LV condensation. The critical line starts at the critical point of the pure 3$_A$ fluid, exhibits a pressure maximum followed by a pressure minimum at lower temperatures, and it continues with a negative slope to high pressures, where it is expected to intersect the solid phase lines. The critical density increases monotonically as the pressure is reduced [a representation of T_c versus η_c is shown in Fig. 8(a)]. Topological changes are not expected for other values of $\epsilon_{AA}^* > 1$, although minor modifications of the critical line may occur. Thus, there is no empty fluid regime in this class of mixtures, as it is pre-empted by LL demixing at low pressures.

2. $0 < \epsilon_{AA}^* < 1, \quad \epsilon_{AB}^* = \epsilon_{BB}^* = 1$

In this class of mixtures it is entropically and energetically favorable to form AB bonds, and therefore these mixtures are expected to exhibit empty fluid behavior. Let us start by reducing the interaction between A patches to $\epsilon_{AA}^* = 0.85$. Temperature-composition phase diagrams at constant pressure are depicted in the second row of Fig. 6. The mixture is completely miscible at pressures above $p_c^{(3)}$. By reducing the pressure below $p_c^{(3)}$, we find that the LV condensation of the pure 3$_A$ fluid at the $x = 0$ axis is shifted to finite values of the composition and ends in an upper critical point. Panel (b$_1$) of Fig. 6 is an example. By contrast to the mixtures investigated previously, the slope of the binodal in the Tx plane is positive, indicating an increase in the stability of the liquid phase when 2$_B$ particles are added to the mixture. The addition of 2$_B$ particles reduces the probability of branching (or equivalently the entropy of bonding) and a negative slope of the binodal signals a decrease in the stability of the liquid phase. Here, however, the loss in the entropy of bonding is overcome by the gain in the bonding energy as the AB bonds are energetically favorable. Note that mixtures where $0 < \epsilon_{BB}^* < 1, \quad \epsilon_{AA}^* = \epsilon_{AB}^* = 1$ (analyzed in Sec. III B 3) are similar but not exactly the same. In that case the bonding energy of the mixture is also minimized by the formation of AB bonds, with respect to BB bonds, but it is higher than the bonding energy of a pure 3$_A$ fluid, whereas in the mixture analyzed in this section ($\epsilon_{AA}^* < 1, \quad \epsilon_{AB}^* = \epsilon_{BB}^* = 1$) it is pos-

sible to achieve mixed states with bonding energy lower than that of the pure 3$_A$ fluid.

As pressure is further reduced, a negative azeotrope appears [see panel (b$_2$) of Fig. 6]. The second LV branch leaving the azeotrope at high composition grows rapidly as the pressure is reduced [panel (b$_3$) in Fig. 6]. This LV branch is bounded by a critical point with critical density and critical temperature that decrease continuously toward zero as the pressure vanishes [see Fig. 8(b)]. Therefore, as expected, the mixture exhibits empty fluid behavior.

Topologically this is again a limiting case of type I mixtures with the addition of a negative azeotrope, usually referred to as type I-A phase equilibria[28] [see the pT projection in panel (b) of Fig. 7].

We proceed by reducing the AA bonding energy to $\epsilon_{AA}^* = 0.5$. Three Tx phase diagrams at representative pressures are depicted in the third row of Fig. 6. The mixture is completely miscible at $p > p_c^{(3)}$. Below $p_c^{(3)}$ there is a range of pressures in which the phase diagram consists only of the LV phase transition, shifted from the $x = 0$ axis [panel (c$_1$) in Fig. 6]. As before, the slope of the binodal is positive. There is a remarkable maximum in the percolation line at temperatures higher than the LV condensation of the pure component. Thus, by increasing the number of particles with two patches it is possible to find re-entrant percolation behavior from a nonpercolated to a percolated fluid and back to to a nonpercolated fluid. The addition of 2$_B$ particles to the mixture reduces branching, but as the AB bonds are energetically favorable, with respect to AA bonds, the probability of branching can, under some circumstances, increase rather than decrease as the composition of 2$_B$ particles increases and re-entrant percolation behavior obtains.

As the pressure is reduced [panel (c$_2$) of Fig. 6] a new two-phase region emerges in the form of a closed loop bounded above (below) by an upper (lower) critical point. It is well inside the percolated region and therefore it is a phase transition between two network fluids or percolated states. The new two-phase region is not connected to the $x = 0$ axis, clearly showing that the condensation is unrelated to the LV condensation of the pure 3$_A$ fluid. As the pressure is further reduced, the distinct two-phase regions merge and, as previously, there is a negative azeotrope [panel (c$_3$) in Fig. 6]. Once the azeotrope appears, a new LV branch grows bounded by a critical point, which moves toward lower temperature and density as the pressure vanishes [see Fig. 8(c)]. The mixture exhibits empty fluid behavior.

Let us focus now on the pT projection of this mixture, represented in Fig. 7(c). It is still a limiting case of type I-A mixtures (type I with an azeotrope). Interestingly, the critical line leaves the critical point of the pure 3$_A$ fluid and goes initially to higher temperatures, a very unusual situation.

3. $\epsilon_{AA}^* = 0, \quad \epsilon_{AB}^* = \epsilon_{BB}^* = 1$

The last set of Tx phase diagrams in Fig. 6 (fourth row) illustrates the extreme case in which A patches do not interact ($\epsilon_{AA}^* = 0$). As a result, none of the two pure fluids undergoes LV condensation. However, the bonding interaction between

dissimilar patches (AB) is present and drives condensation at pressures below $p^{(+)} \approx 2.92 \times 10^{-5} \epsilon / v_s$. Slightly below $p^{(+)}$ [panel (d$_1$) of Fig. 6] a closed miscibility gap grows inside the percolated region. Well below $p^{(+)}$ [panels (d$_2$) and (d$_3$) of Fig. 6] there is a negative azeotrope with two LV branches bounded by critical points. As the pressure vanishes, both critical temperatures tend to zero, but the critical density behaves differently in each branch [see Fig. 8(d)]. The critical point rich in 2_B particles exhibits empty fluid behavior, while the critical point rich in 3_A particles tends asymptotically to $\eta_c \to 0.007$.

The behavior is analogous to the mixture with $\epsilon_{AA}^* = 0.5$ with the absence of the LV branch connected to the pure 3_A fluid condensation. It is not possible to classify this mixture following van Konynenburg and Scott[28] as neither of the pure fluids has LV condensation. The critical line in the pT projection [see Fig. 7(d)] forms a closed loop starting and ending at $p \to 0$ and $T \to 0$ where we have found two different solutions.

D. $2_B - 3_A$ mixtures: $\epsilon_{AA} = \epsilon_{BB}$

Finally, we analyze mixtures with $\epsilon_{AA}^* = \epsilon_{BB}^*$. Representative examples of Tx phase diagrams at $p_1^* = pv_s/\epsilon = 1.05 \times 10^{-4}$ are plotted in Fig. 9, the pressure–temperature projections are depicted in Fig. 10, and the properties of the critical points are shown in Fig. 11.

1. $\epsilon_{AB}^* > 1$, $\epsilon_{AA}^* = \epsilon_{BB}^*$

In this case AB bonds are energetically favorable with respect to both AA or BB bonds, and therefore there is no LL demixing at low temperatures.

The Tx phase diagrams are qualitatively the same as those of the reference $2_A - 3_A$ mixture. An example is plotted in panel (a) of Fig. 9 for $\epsilon_{AB}^* = 1.1$ at p_1^*. It should be compared to the phase diagram of the $2_A - 3_A$ reference mixture depicted in panel (b$_1$) of Fig. 3. At constant pressure, the LV two-phase region shrinks as the strength of the interaction between dissimilar patches increases, and the critical point moves toward higher temperature and lower composition. These mixtures are limiting cases of type I (Fig. 10), and, as expected, the critical packing fraction and the critical temperature tend to zero as the pressure vanishes (Fig. 11). In other words, the mixture exhibits empty fluid behavior.

Changes in the topology of the phase diagram (as the appearance of negative azeotropes) may arise if the bonding interaction between dissimilar patches is much stronger than the interaction between identical patches: $\epsilon_{AB}^*/\epsilon_{\alpha\alpha}^* \gg 1$, $\alpha = A, B$. Nevertheless, as far as the critical properties at low pressure are concerned, no changes are expected to occur.

2. $0 \leq \epsilon_{AB}^* < 1$, $\epsilon_{AA}^* = \epsilon_{BB}^*$

A small decrease in the AB bonding interaction drives phase separation at low temperature, pre-empting the empty fluid regime. We have plotted two phase diagrams at the same pressure (p_1^*) in Fig. 9 for: $\epsilon_{AB}^* = 0.955$ in panel (b) and

TABLE I. Summary of the phase behavior of $2_B - 3_A$ mixtures: The bonding energy that characterizes the mixture (the other two are set to one), the stability of empty fluids and the topological classification of the mixture phase diagram.

Mixture	Empty fluids	Type	Section
$\epsilon_{BB}^* > 1$	no	III	III B 1
$0 < \epsilon_{BB}^* < 1$	yes	I	III B 3
$\epsilon_{BB}^* = 0$	no	I	III B 2
$\epsilon_{AA}^* > 1$	no	III	III C 1
$0 < \epsilon_{AA}^* < 1$	yes	I-A	III C 2
$\epsilon_{AA}^* = 0$	yes	–	III C 3
$\epsilon_{AB}^* > 1$	yes	I	III D 1
$0 < \epsilon_{AB}^* < 1$	no	III	III D 2
$\epsilon_{AB}^* = 0$	no	III	III D 2

$\epsilon_{AB}^* = 0$ in panel (c). For bonding strengths $\epsilon_{AB}^* \lesssim 1$ there are two regions of phase separation (LL demixing bounded by an upper critical point at low temperatures, and LV condensation bounded by a lower critical point at high temperatures) at pressures below the critical pressure of the pure 3_A fluid (b). When $\epsilon_{AB}^* \ll 1$, both regions merge into a single two-phase region without critical points below $p_c^{(3)}$, see, for example, panel (c). In both cases, at pressures above $p_c^{(3)}$, LL demixing is always present bounded by an upper critical point. These mixtures are limiting cases of type III mixtures (see Fig. 10). The strength of the AB interaction leads to slight changes of the critical line. Note, for example, the slope of the critical line at high pressures: positive when $\epsilon_{AB}^* \ll 1$ and negative when $\epsilon_{AB}^* \lesssim 1$.

IV. CONCLUSIONS

We have carried out a systematic analysis of binary mixtures of patchy particles with two patches of type B and three patches of type A, focusing on the empty fluid behavior discovered in one of these mixtures.[11,12] We have found a rich phase behavior with closed miscibility gaps, liquid–liquid demixing, negative azeotropes, and, from a topological point of view, three different types of mixtures: type I, I-A, and III. The main results are summarized in Table I.

We have found that liquid–liquid demixing, at low temperatures and pressures, is the primary mechanism that preempts the empty fluid regime in some of these mixtures. LL demixing is always present when unlike (AB) bonds are weaker than at least one of the other two bonds between particles of the same species (AA or BB bonds). These mixtures are limiting cases of type III. Within this class the detailed phase behavior depends on the values of the bonding energies. For example, the slope of the critical line in the pT projection, the appearance of closed miscibility gaps, or the asymptotic values of the critical temperature and critical concentration as the pressure increases, are controlled by the specific values of the bonding energies.

The mixtures exhibit empty fluid behavior if the AB bonds are stronger than at least one of the other two. These mixtures are limiting cases of type I or type I-A (type I with the addition of a negative azeotrope).The most interesting

case occurs in mixtures with bonding strengths $\epsilon_{BB}^* = \epsilon_{AB}^*$ and $\epsilon_{AA}^* \ll 1$. In these mixtures there is a negative azeotrope and the critical line goes initially to the temperatures above that of the pure 3_A fluid.

There is only one case where AB bonds are energetically favorable and the mixture does not exhibit empty fluid behavior: the mixture with $\epsilon_{AB} = \epsilon_{AA}$ and $\epsilon_{BB} = 0$. In this case the absence of bonding between particles with two patches precludes the empty liquid regime. In fact, near the critical point of the mixture there is coexistence between two network fluids with finite packing fractions as the pressure vanishes. This behavior is similar to that found previously[21] for $2_A - 5_A$ binary mixtures (i.e., mixtures of particles with two and five identical patches) where the entropy of bonding drives the liquid–liquid demixing pre-empting the liquid–vapor phase transition.

In a previous study[21] we found that the driving force for the topological change in the phase diagram of mixtures with a single bonding energy is the difference in the bonding entropy associated with bonds between like and unlike particles. It is desirable to address this question in more detail by investigating mixtures of particles with different diameters, and/or, different types of bonding sites in such a manner that both fluids are constrained to have similar values of the critical pressure and temperature. In that context, the present study is a step toward elucidating the competition between the bonding entropy and the bonding energy in the determination of the topology of the phase diagrams of binary mixtures.

Binary mixtures of particles with different types of bonding sites are also crucial to the investigation of a wide range of structured fluids, with different macroscopic properties, including stable bicontinuous gels.[32,33] This is an immediate goal that will be addressed in future work.

Finally, a word about the absolute stability of the fluid phases reported in this paper. Although at low pressures and low (but finite) temperatures we expect the fluid to be absolutely stable, it is clear that solid phases will intervene and pre-empt some of the high pressure and/or low temperature features of the phase diagrams reported here. The calculation of solid phase diagrams is much more complicated but progress has been reported recently, including the ground state analysis of binary mixtures of low-functionality patchy particles in two dimensions.[34,35]

ACKNOWLEDGMENTS

[1] P. N. Pusey, J. Phys. Condens. Matter **20**, 494202 (2008).

[2] E. Zaccarelli, J. Phys. Condens. Matter **19**, 323101 (2007).

[3] M. E. Leunissen, C. G. Christova, A.-P.Hynninen, C. P. Royall, A. I. Campbell, A. Imhof, M. Dijkstra, R. van Roij, and A. van Blaaderen, Nature (London) **437**, 235 (2005).

[4] A.-P. Hynninen, J. H. J. Thijssen, E. C. M. Vermolen, M. Dijkstra, and A. van Blaaderen, Nature Mater. **6**, 202 (2007).

[5] A. Stradner, G. Foffi, N. Dorsaz, G. Thurston, and P. Schurtenberger, Phys. Rev. Lett. **99**, 198103 (2007).

[6] A. B. Pawar and I. Kretzschmar, Macromol. Rapid Commun. **31**, 150 (2010).

[7] Q. Chen, S. C. Bae, and S. Granick, Nature (London) **469**, 381 (2011).

[8] Q. Chen, J. K. Whitmer, S. Jiang, S. C. Bae, E. Luijten, and S. Granick, Science **331**, 199 (2011).

[9] S. Sacanna, W. T. M. Irvine, P. M. Chaikin, and D. J. Pine, Nature (London) **464**, 575 (2010).

[10] S. Sacanna, W. T. M. Irvine, L. Rossi, and D. J. Pine, Soft Matter **7**, 1631 (2011).

[11] E. Bianchi, J. Largo, P. Tartaglia, E. Zaccarelli, and F. Sciortino, Phys. Rev. Lett. **97**, 168301 (2006).

[12] E. Bianchi, P. Tartaglia, E. Zaccarelli, and F. Sciortino, J. Chem. Phys. **128**, 144504 (2008).

[13] B. Ruzicka, E. Zaccarelli, L. Zulian, R. Angelini, M. Sztucki, A. Moussaïd, T. Narayanan, and F. Sciortino, Nature Mater. **10**, 56 (2011).

[14] M. S. Wertheim, J. Stat. Phys. **35**, 35 (1984).

[15] M. S. Wertheim, J. Stat. Phys. **35**, 19 (1984).

[16] M. S. Wertheim, J. Stat. Phys. **42**, 459 (1986).

[17] M. S. Wertheim, J. Stat. Phys. **42**, 477 (1986).

[18] P. J. Flory, J. Am. Chem. Soc. **63**, 683 (1941).

[19] W. H. Stockmayer, J. Chem. Phys. **11**, 45 (1943).

[20] P. J. Flory, *Principles of Polymer Chemistry* (Cornell University Press, Ithaca, 1981).

[21] D. De las Heras, J. M. Tavares, and M. M. Telo da Gama, "Phase diagrams of binary mixtures of patchy colloids with distinct numbers of patches," (2010) (submitted), e-print arXiv:1012.3605v1.

[22] J. M. Tavares, P. I. C. Teixeira, and M. M. Telo da Gama, Phys. Rev. E **80**, 021506 (2009).

[23] J. M. Tavares, P. I. C. Teixeira, and M. M. Telo da Gama, Mol. Phys. **107**, 453 (2009).

[24] J. M. Tavares, P. I. C. Teixeira, M. M. T. da Gama, and F. Sciortino, J. Chem. Phys. **132**, 234502 (2010).

[25] J. M. Tavares, P. I. C. Teixeira, and M. M. Telo da Gama, Phys. Rev. E **81**, 010501(R) (2010).

[26] J. Russo, J. M. Tavares, P. I. C. Teixeira, M. M. Telo da Gama, and F. Sciortino, Phys. Rev. Lett. **106**, 085703 (2011).

[27] W. G. Chapman, G. Jackson, and K. E. Gubbins, Mol. Phys. **65**, 1057 (1988).

[28] P. H. Van Konynenburg and R. L. Scott, Philos. Trans. R. Soc. London Ser. A **298**, 495 (1980).

[29] N. F. Carnahan and K. E. Starling, J. Chem. Phys. **51**, 635 (1969).

[30] J. Rowlinson and F. L. Swinton, *Liquids and Liquid Mixtures* (Butterworths, England, 1982).

[31] There is one exception, when $\epsilon_{AA} = 0$, none of the pure fluids undergoes LV condensation, and therefore it is not possible to classify this mixture within the standard classification of van Konynenburg and Scott. See also Ref. 28.

[32] A. Goyal, C. K. Hall, and O. D. Velev, J. Chem. Phys. **133**, 064511 (2010).

[33] A. Goyal, C. K. Hall, and O. D. Velev, Soft Matter **6**, 480 (2010).

[34] G. Doppelbauer, E. Bianchi, and G. Kahl, J. Phys. Condens. Matter **22**, 104105 (2010).

[35] J. P. K. Doye, A. A. Louis, I.-C. Lin, L. R. Allen, E. G. Noya, A. W. Wilber, H. C. Kok, and R. Lyus, Phys. Chem. Chem. Phys. **9**, 2197 (2007).